

Extended MCDHF calculations of energy levels and transition data for N I

M. C. LI,¹ W. LI,² P. JÖNSSON,³ A. M. AMARSI,⁴ AND J. GRUMER⁴

¹*School of Electronic Information and Electrical Engineering, Huizhou University, Huizhou, China 516007*

²*Key Laboratory of Solar Activity, National Astronomical Observatories, Chinese Academy of Sciences, Beijing 100012, China*

³*Department of Materials Science and Applied Mathematics, Malmö University, SE-205 06 Malmö, Sweden*

⁴*Theoretical Astrophysics, Department of Physics and Astronomy, Uppsala University, Box 516, SE-751 20 Uppsala, Sweden*

ABSTRACT

Accurate and extensive atomic data are essential for spectroscopic analyses of stellar atmospheres and other astronomical objects. We present energy levels, lifetimes, and transition probabilities for neutral nitrogen, the sixth most abundant element in the cosmos. The calculations employ the fully relativistic multiconfiguration Dirac-Hartree-Fock and relativistic configuration interaction methods, and span the 103 lowest states up to and including $2s^22p^25s$. Our theoretical energies are in excellent agreement with the experimental data, with an average relative difference of 0.07%. In addition, our transition probabilities are in good agreement with available experimental and theoretical data. We further verify the agreement of our data with experimental results via a re-analysis of the solar nitrogen abundance, with the results from the Babushkin and Coulomb gauges consistent to 2% or 0.01 dex. We estimated the uncertainties of the computed transition data based on a statistical analysis of the differences between the transition rates in Babushkin and Coulomb gauges. Out of the 1701 computed electric dipole transitions in this work, 83 (536) are associated with uncertainties less than 5% (10%).

Keywords: atomic data; solar abundances

1. INTRODUCTION

Nitrogen is the sixth most abundant element in the Universe (Asplund et al. 2021), and its abundance is an important diagnostic in the study of the structure and evolution of stars (Hirschi 2007; Aerts et al. 2014; Maeder et al. 2014), globular clusters (Spite et al. 2022), and galaxies (Belfiore et al. 2017; Masseron & Gilmore 2015; Schiavon et al. 2017; Vincenzo & Kobayashi 2018; Esteban et al. 2020). Nitrogen abundance measurements in the atmospheres of stars via stellar spectroscopy are critical in this endeavour. In hot stars of spectral types O, B, A, and F, near-infrared and infrared N I lines arising from transitions involving the configurations $2p^2(^3P)3s$, $2p^2(^3P)3p$, $2p^2(^1D)3s$, $2p^2(^3P)3d$, and $2p^2(^1D)3p$ are typically used (Takeda & Takada-Hidai 1995; Przybilla & Butler 2001). Several weak N I lines can also be detected in cooler stars (Kolecki & Wang 2022), including the Sun; these have been used to inform the solar nitrogen abundance, together with molecular diagnostics such as NH and CN (Lambert 1978; Grevesse et al. 1990; Amarsi et al. 2020, 2021).

High quality atomic data for N I are indispensable for reliable stellar spectroscopic analyses. During the past 30 years, several tens of experimental and theoretical studies of transition data have been carried out for N I. The complete lists of published papers on these measurements and calculations can be retrieved from the NIST Atomic Transition Probability Bibliographic database (Kramida & Fuhr 2010). For example, on the experimental side, using a wall-stabilized arc source, measurements of transition probabilities and line strengths for visible and infrared lines, originating from transition arrays $3s$ - $3p$, $3s$ - $4p$, $3p$ - $3d$, and $4d$ - $5s$ were performed by Musielok et al. (1995), Bačlawski et al. (2002), Bačlawski & Musielok (2010, 2008), and Bridges & Wiese (2010). The relative uncertainties of these measurements were claimed to be no more than 15%. Using the same method, Goldbach & Nollez (1991) and Goldbach

et al. (1992) measured the oscillator strengths for 19 lines in the 90–125 nm region and 18 lines in the 120–200 nm region, respectively. There are also a number of experimental measurements of lifetimes and oscillator strengths using various techniques (Bengtsson et al. 1992; Dumont et al. 1974; Catherinot & Sy 1979; Copeland et al. 1987; Bromander et al. 1978).

On the theoretical side, a few tens of theoretical studies of excitation energies and transition data for N I have been reported. For example, Hibbert et al. (1991) calculated the excitation energies and oscillator strengths for a number of dipole-allowed and intercombination transitions between doublet and quartet states with the configuration interaction method. Using the multiconfigurational Hartree-Fock and Breit-Pauli (MCHF-BP) method, calculations of oscillator strengths for N I have been performed by Tong et al. (1994), Tachiev & Froese Fischer (2002) and Froese Fischer & Tachiev (2004). Tong et al. (1994) only reported oscillator strengths of transitions among low-lying quartet states, whereas Tachiev & Froese Fischer (2002) and Froese Fischer & Tachiev (2004) calculated energy levels and lifetimes for all levels up to $2s^22p^23d$, as well as transition data between these levels. Among these theoretical results, the MCHF-BP values (Tachiev & Froese Fischer 2002; Froese Fischer & Tachiev 2004) are in overall better agreement with experimental results than the others. More recently, Bautista et al. (2022) calculated the gf -values of the two lines at 8683 Å and 8629 Å, which are diagnostics of the solar nitrogen abundance, using a combination of different methods, i.e. AUTOSTRUCTURE based on the Thomas-Fermi-Dirac-Amaldi central potential, pseudo-relativistic Hartree-Fock, and multiconfiguration Dirac-Hartree-Fock (MCDHF) methods.

In the present work we perform large-scale ab initio calculations of excitation energies and electric dipole (E1) transition parameters (transition rates, line strengths and weighted oscillator strengths) for the 103 lowest states belonging to the $2s^22p^3$, $2s2p^4$, $2s^22p^2nl$ ($n = 3, 4$, $l = s, p, d, f$), and $2s^22p^25s$ configurations in N I. Calculations are based on fully relativistic MCDHF and configuration interaction (RCI) methods, as implemented in the general-purpose relativistic atomic structure package GRASP2018¹ (Froese Fischer et al. 2019).

2. THEORY AND COMPUTATIONS

2.1. Theory

In the MCDHF method (Froese Fischer et al. 2016) as implemented in the GRASP code, the atomic eigenstate is represented by an atomic state expressed as a linear combination of configuration state functions (CSFs) with equal parity P and angular momentum quantum numbers JM :

$$\Psi(\gamma P J M) = \sum_i c_i \Phi(\gamma_i P J M) \quad (1)$$

The CSFs are jj -coupled many-electron functions built from antisymmetrized products of single-electron Dirac orbitals. The quantities c_i and γ_i are, respectively, the mixing coefficient and additional labeling needed to uniquely specify each CSF. The radial parts of the Dirac orbitals and the expansion coefficients c_i of the targeted states are all optimized to self-consistency by solving the MCDHF equations, which are derived by applying the variational principle on the weighted average energy of the targeted states. Higher-order electron-electron interactions, such as the frequency-independent Breit interaction and leading quantum electrodynamical effects in the form of the self-energy (SE) and the screened vacuum polarization (VP), are included in the subsequent relativistic configuration interaction (RCI) calculations using the orbital basis from the MCDHF optimization (Grant 2007).

The E1 transition data (transition probabilities and weighted oscillator strengths) between two states $\gamma' P' J'$ and $\gamma P J$ are expressed in terms of reduced matrix elements of the electric dipole transition operator $T^{(1)}$. From Equation 1, these matrix elements can be written as

$$\langle \Psi(\gamma P J) \| T^{(1)} \| \Psi(\gamma' P' J') \rangle = \sum_{i,j} c_i c'_j \langle \Phi(\gamma_i P J) \| T^{(1)} \| \Phi(\gamma'_j P' J') \rangle. \quad (2)$$

Here, c_i and c_j are, respectively, the expansion coefficients of the CSFs for the upper and lower states. Using the Brink-and-Satchler convention, the reduced matrix elements in Equation 2 can be expressed in terms of spin-angular coefficients $d_{ab}^{(1)}$ and operator strengths as

$$\langle \Phi(\gamma_i P J) \| T^{(1)} \| \Phi(\gamma'_j P' J') \rangle = \sum_{a,b} d_{ab}^{(1)} \langle n_a l_a j_a \| t^{(1)} \| n_b l_b j_b \rangle \quad (3)$$

¹ See also the open-source GitHub repository maintained by the CompAS collaboration: <https://github.com/compas/grasp>.

where

$$\langle n_a l_a j_a || t^{(1)} || n_b l_b j_b \rangle = \left(\frac{(2j_b + 1)\omega}{\pi c} \right)^{1/2} (-1)^{j_a - 1/2} \begin{pmatrix} j_a & 1 & j_b \\ \frac{1}{2} & 0 & -\frac{1}{2} \end{pmatrix} \overline{M}_{ab} \quad (4)$$

Here, n, l, j are, respectively, the principal, orbital and angular quantum numbers of spin-orbitals a and b , $\hbar\omega$ is the electromagnetic energy, and \overline{M}_{ab} is the radiative transition integral defined by Grant (1974). For electric type multipoles, the \overline{M}_{ab} integral can be written as $\overline{M}_{ab}(G) = \overline{M}_{ab}^e + G\overline{M}_{ab}^l$ (see equation 4.10 in Grant (1974)), where \overline{M}_{ab}^e is the Coulomb gauge integral, \overline{M}_{ab}^l the longitudinal part and G the gauge parameter. Two familiar choices, corresponding to the velocity and length operator forms in non-relativistic theory, are the Coulomb ($G = 0$) and Babushkin ($G = \sqrt{2}$) gauges.

The agreement between transition rates in the Coulomb gauge (A_C) and the Babushkin gauge (A_B), is often taken as an internal indicator of accuracy of calculated data, especially when there are no experimental results available. The relative differences between transition rates A_B and A_C , dT , is defined as (Froese Fischer 2009; Ekman et al. 2014)

$$dT = \frac{|A_B - A_C|}{\max(A_B, A_C)}. \quad (5)$$

It should be emphasized that dT gives an estimation of the uncertainty for groups of lines in a statistical manner.

2.2. Computational Schemes

Calculations were performed in the extended optimal level (EOL) scheme (Dyall et al. 1989) for the weighted average of the even and odd parity states. These states belong to the $\{2s^2p^4, 2s^22p^2nl(n = 3, 4, l = s, d), 2s^22p^25s\}$ even configurations and the $\{2s^22p^3, 2s^22p^2nl(n = 3, 4, l = p, f)\}$ odd configurations. These target configurations are included in the multireference (MR) set used in the MCDHF calculations.

Following the CSF generation strategies used by, e.g. Papoulia et al. (2019) and Li et al. (2021), the MCDHF calculations were based on CSF expansions for which we impose restrictions on the orbital excitations from the deeper subshells. The CSFs are generated and systematically enlarged through single and double (SD) excitation from subshells occupied in the predefined MR configurations to an active set (AS) of orbitals in a step-by-step manner (Olsen et al. 1988; Stuesson et al. 2007; Froese Fischer et al. 2016).

In the present calculations, the orbitals in the $n = 1$ shell of the MR configurations are defined as core orbitals. The remaining orbitals are defined as valence orbitals. Based on these definitions, the valence-valence (VV) electron correlations are included in the calculation by allowing SD excitations from the valence orbitals to active sets of orbitals, with the restriction that there is at most one excitation from the $n = 2$ shell.

With an MCDHF orbital basis at hand, the MR set was then further extended and applied in a subsequent RCI calculation, as shown in Table 1. The extended MR set comprises configurations that give rise to LSJ -coupled CSFs with weights larger than 0.05. Core-valence (CV) electron correlation effects were taken into account by allowing SD substitutions from the valence shells and the $1s^2$ core of the configurations in the extended MR, with the restriction that at most one excitation is allowed from $1s^2$, to the final active set, $\{11s, 10p, 10d, 10f, 7g, 6h\}$. The numbers of CSFs in the final even and odd state expansions were, respectively, 13 431 751 and 17 662 086, distributed over the different J symmetries.

Table 1. Summary of the active space construction. The configurations in the second and third columns, respectively, represent the target states and the extended target MR set in RCI calculation. N_{CSFs} denotes the number of CSFs in the total expansion for the even and odd parity states in the final RCI calculation.

Parity	MR	Extended MR in RCI	N_{CSFs}
Even	$2s^2p^4, 2s^22p^23s$	$2s^2p^3np(3 \leq n \leq 5)$	13 431 751
	$2s^22p^23d, 2s^22p^24s$	$2p^4nl(3 \leq n \leq 5, l = s, d)$	
	$2s^22p^24d, 2s^22p^25s$		
Odd	$2s^22p^3, 2s^22p^23p$	$2s^2p^3nl(3 \leq n \leq 5, l = s, d)$	17 662 086
	$2s^22p^24p, 2s^22p^24f$	$2p^44f, 2s^2p^4np(3 \leq n \leq 5)$	

3. RESULTS AND DISCUSSION

3.1. *Energies and Lifetimes*

The calculated energies and corresponding wave function composition in LS -coupling for the lowest 103 states are displayed in Table 2. The labelling of the eigenstates is defined by the LSJ -coupled CSF with the largest expansion coefficient resulting from the transformation from jj -coupling to LSJ -coupling using the method by Gaigalas et al. (2017). We note that LSJ -coupling might not be the best representation to describe the states associated to the $2s^2 2p^2 4f$ configuration and that the National Institute of Standards and Technology Atomic Spectra Database (NIST-ASD) (Kramida et al. 2021) adopts JK -coupling in their labeling of these. The corresponding experimental energies provided via NIST-ASD, as well as radiative lifetimes in both Babushkin (B) and Coulomb (C) forms are also included in Table 2. When compared with energies from NIST-ASD, we noticed two pairs of levels, #74-75 ($2p^2 4d \ ^4P_{5/2}$ and $\ ^2F_{5/2}$) and #80-82 ($2p^2 4d \ ^4D_{1/2}$ and $\ ^4P_{1/2}$), being inverted based on the energy ordering. A closer inspection of the LS -composition reveals that these states are strongly mixed, the leading percentages being about 40-60% and the second components about 30-40%, and they might be less accurately described by the conventional labelling based on the expansion coefficients. Since a close agreement of the computed energies with the NIST-ASD values being observed for the other levels, we matched the corresponding two pairs of levels with experimental energies based on the energy ordering within each symmetry. Note that the labelling of these two pairs of levels, i.e. #74-75 and #80-82, given in the second column of Table 2 are inverted compared to that of the NIST-ASD data.

Table 2. Energies (in cm^{-1}) and lifetimes (in s) in both the Babushkin (τ_B) and Coulomb (τ_C) gauges for the lowest 103 levels of N I. Energy levels are given relative to the ground state and compared with results from NIST-ASD (Kramida et al. 2021). The labelling in the second column is defined by the composition with the largest expansion coefficient given in the third column. This table is available in its entirety in electronic form.

No.	State	LS -composition	E_{RCI}	E_{NIST}	ΔE	τ_B	τ_C
1	$2s^2 2p^3 \ ^4S_{3/2}^\circ$	0.91	0	0.000	0		
2	$2s^2 2p^3 \ ^2D_{5/2}^\circ$	0.89	19426	19224.464	-201		
3	$2s^2 2p^3 \ ^2D_{3/2}^\circ$	0.89	19435	19233.177	-201		
4	$2s^2 2p^3 \ ^2P_{1/2}^\circ$	$0.85 + 0.03 2p^5 \ ^2P^\circ$	29142	28838.920	-304		
5	$2s^2 2p^3 \ ^2P_{3/2}^\circ$	$0.85 + 0.03 2p^5 \ ^2P^\circ$	29143	28839.306	-303		
6	$2s^2 2p^2(^3P) 3s \ ^4P_{1/2}$	$0.82 + 0.12 2s 2p^4 \ ^4P$	83332	83284.070	-48	2.44E-09	2.44E-09
7	$2s^2 2p^2(^3P) 3s \ ^4P_{3/2}$	$0.82 + 0.12 2s 2p^4 \ ^4P$	83366	83317.830	-48	2.42E-09	2.42E-09
8	$2s^2 2p^2(^3P) 3s \ ^4P_{5/2}$	$0.81 + 0.12 2s 2p^4 \ ^4P$	83413	83364.620	-49	2.40E-09	2.39E-09
9	$2s^2 2p^2(^3P) 3s \ ^2P_{1/2}$	0.95	86187	86137.350	-50	2.10E-09	2.10E-09
10	$2s^2 2p^2(^3P) 3s \ ^2P_{3/2}$	0.95	86270	86220.510	-50	2.10E-09	2.10E-09
...

NOTE—The third column gives wave function composition (up to three LS -components with a fractional contribution of > 0.02 of the total wave function) in LS -coupling. ΔE donate the differences between the MCDHF/RCI calculated values and the compiled values from NIST-ASD, i.e. $\Delta E = E_{\text{NIST}} - E_{\text{RCI}}$. Note that the labelling of the two level pairs, #74-75 and #80-82, given in the second column are inverted compared to that of the NIST-ASD data.

The results of the comparison of computed energy levels in this work with experimental values are shown in Fig. 1. As seen in the left panel of Fig. 1, our computed energies agree very well with the NIST compiled experimental energies with an average relative difference of 0.07%. The largest relative difference between theory and experiment is 1.05% for the levels belonging to doublet terms of the $2s^2 2p^3$ ground configuration. For the remaining 98 levels, the relative differences of the computed excitation energies are much smaller, with an average of 0.03%. The right panel of Fig. 1 shows the energy differences between NIST-ASD values and the present computed data, $\Delta E = E_{\text{NIST}} - E_{\text{RCI}}$, plotted against the excitation energies, E_{RCI} . We can see that the largest error happens for the ground levels, which are about 200-300 cm^{-1} higher than the NIST-ASD values. The root mean square (rms) of the ΔE values is about 67 cm^{-1} . When the computational excitation energies are corrected with the linear fitting results, the rms of the ΔE values decreased to 28 cm^{-1} , with a systematic error of 0.26% of the excitation energies.

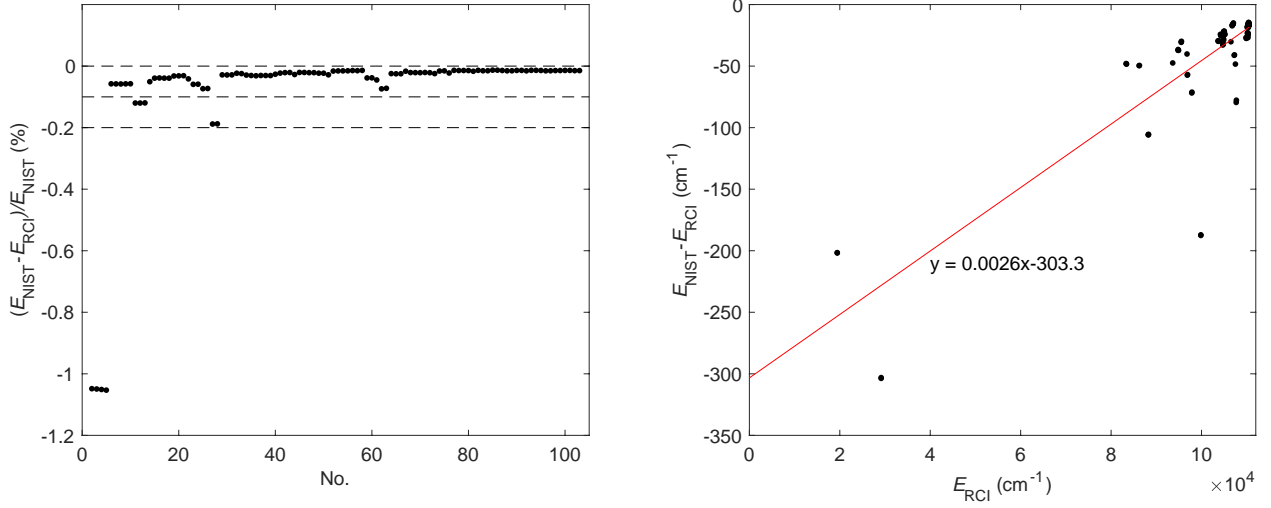


Figure 1. Comparison of the current computed excitation energies with the values available in the NIST-ASD. The left panel shows the relative difference for each level, while the right panel shows the absolute difference along with present computed energies. The dashed lines in the left panel, from upper to lower, indicate the 0.2%, 0.1% and 0.0% relative discrepancies, respectively. The red solid line in the right panel is the linear fit to the scatter data shown in the figure.

In Table 3 we compare the lifetimes from present calculations with other theoretical results and experimental values, when available. The calculated lifetimes in Babushkin and Coulomb forms are in agreement within 2.6%. Compared with the theoretical results from CIV3 calculations by Hibbert et al. (1991) and MCHF-BP calculations by Froese Fischer & Tachiev (2004), excellent agreement is observed for 7 out of 8 lifetime values, with the relative difference between each two of them being less than 7%. For the $2p^2(^3P)4s\ ^2P$ term, the lifetime value from the present work is about a factor of two smaller than the CIV3 results, but in agreement with the MCHF-BP value, with the relative difference less than 6% and in better agreement with the experimental value from Dumont et al. (1974). Good agreement is also observed between computed and experimental lifetime values, except for the $2p^2(^3P)3p\ ^4P_{5/2}^o$ and $2p^2(^3P)4s\ ^2P$ levels. For the $2p^2(^3P)3p\ ^4P_{5/2}^o$ level, all the theoretical lifetimes differ substantially from the experimental values and the two experimental values by Bromander et al. (1978) and Désesquelles (1970) differ by 30% with each other. On the contrary, the theoretical results obtained from three different methods, i.e. MCDHF, MCHF-BP and CIV3, are in good agreement within 8%. For the $2p^2(^3P)4s\ ^2P$ state, all the theoretical values are larger than the experimental result obtained from Dumont et al. (1974). Our predicted lifetime is in good agreement with that from MCHF-BP calculation (Froese Fischer & Tachiev 2004), while the value from Hibbert et al. (1991) is larger than the others. New experimental measurements of lifetimes would therefore be welcome for these levels.

3.2. Transition parameters

The E1 transition data, such as wavelengths (λ), transition rates (A), line strengths (S), weighted oscillator strengths (gf) in Babushkin gauge, are listed in Table 4. We note that the wavelengths in Table 4 are computed from the experimental energy levels compiled in the NIST-ASD and the transition parameters A and gf are also adjusted to the NIST-ASD wavelength values.

As mentioned in section 2.1, the dT values can be used to assess the accuracy of the transition parameters. The former are shown in the last column of Table 4. We also investigated the distribution of dT values with respect to the magnitude of the transition rates A . In Table 5, the transitions are organized in five groups based on the magnitude of the A values and the statistical results of dT values, i.e. the mean value $\langle dT \rangle$ and the corresponding standard deviations σ , are given for each group. $\langle dT \rangle$ and σ are defined as

$$\langle dT \rangle = \frac{\sum_{i=1}^n dT_i}{n} \quad (6)$$

$$\sigma = \sqrt{\frac{\sum_{i=1}^n (dT_i - \langle dT \rangle)^2}{(n-1)}} \quad (7)$$

Table 3. Comparison of the experimental and calculated lifetimes (in ns, B = Babuskin form and C = Coulomb form). The lifetime of a term is the mean value of the lifetime corresponding to the different J values. The notation for experimental values, e.g., 44(2) implies 44 ± 2 .

State or term	This work		Other calculations	Experiments
	B	C		
$2p^2(^3P)3p\ ^4D_{7/2}$	39.8	40.3	37.9^a ; 37.12^b	$44(2)^c$; $43(3)^d$
$2p^2(^3P)3p\ ^4S_{3/2}$	25.3	25.5	24.1^a ; 23.26^b	$26.0(1.5)^c$; $23.3(2.3)^e$
$2p^2(^3P)3p\ ^4P_{5/2}$	33.4	33.9	31.6^a ; 31.22^b	39^f ; $55(5)^g$
$2s2p^4\ ^4P$	6.90	6.75	6.77^a ; 7.14^b	$7.3(0.7)^h$; $7.4(0.4)^i$; $7.0(0.2)^j$ $7.1(0.4)^f$; $5.5(1.5)^k$; $9.9(1.0)^l$; $7.2(0.7)^m$
$2p^2(^3P)3s\ ^4P$	2.42	2.42	2.48^a ; 2.59^b	$2.35(0.23)^{f,h}$; $2.4(0.1)^j$; $2.2(0.4)^l$; $2.5(0.3)^m$
$2p^2(^3P)3s\ ^2P$	2.10	2.10	2.13^a ; 1.95^b	$1.9(0.3)^{h,m}$; $2.3(0.4)^h$; $2.2(0.1)^j$ $1.7(0.4)^l$; $1.9(0.4)^l$; $2.28(0.2)^f$
$2p^2(^1D)3s\ ^2D$	2.57	2.58	2.44^a ; 2.44^b	$2.27(0.3)^h$; $2.26(0.3)^h$; $2.65(0.3)^f$ $2.6(0.1)^j$; $2.5(0.4)^k$; $2.2(0.3)^m$
$2p^2(^3P)4s\ ^2P$	8.52	8.75	8.02^a ; 18.8^b	6.2^h

NOTE—^a Froese Fischer & Tachiev (2004); ^b Hibbert et al. (1991); ^c Bengtsson et al. (1992); ^d Copeland et al. (1987); ^e Catherinot & Sy (1979); ^f Désesquelles (1970); ^g Bromander et al. (1978); ^h Dumont et al. (1974); ⁱ Smith et al. (1970); ^j Berry et al. (1971); ^k Mallow & Burns (1972); ^l Hutchison (1971); ^m Lawrence & Savage (1966)

Table 4. Electric dipole transition data for N I from present calculations. Upper and lower states, wavelength in vacuum, $\lambda_{vac.}$, transition probability, A , line strength, S (in unit au of $a_0^2e^2$), weighted oscillator strength, $\log(gf)$, together with the relative difference between two gauges of A values, dT , and Accuracy class, Acc., are shown in the table. The wavelengths and all the transition parameters are adjusted to the NIST-ASD Ritz wavelength values. The accuracy class, Acc., is given by: A (Uncertainty $\leq 3\%$), B+ ($3\% < \text{Uncertainty} \leq 7\%$), B ($7\% < \text{Uncertainty} \leq 10\%$), C+ ($10\% < \text{Uncertainty} \leq 18\%$), C ($18\% < \text{Uncertainty} \leq 25\%$), D+ ($25\% < \text{Uncertainty} \leq 40\%$), D ($40\% < \text{Uncertainty} \leq 50\%$), and E ($50\% > \text{Uncertainty}$). This table is available in its entirety in electronic form.

Upper	Lower	λ (Å)	A_B (s^{-1})	A_C (s^{-1})	$\log(gf)_B$	$\log(gf)_C$	S_B	S_C	dT	Acc.	
										$dT\&$	$gf_{\text{RCI}\&}$
										A	$gf_{\text{NIST-ASD}}$
$2s^2\ 2p^2(^3P)4d\ ^2D_{5/2}$	$2s^2\ 2p^3\ ^4S_{3/2}^o$	905.221	1.444E+06	1.623E+06	-2.973	-2.922	3.172E-03	3.565E-03	0.110	C+	C
$2s^2\ 2p^2(^3P)4d\ ^2D_{3/2}$	$2s^2\ 2p^3\ ^4S_{3/2}^o$	905.411	4.649E+05	5.202E+05	-3.641	-3.592	6.813E-04	7.623E-04	0.106	C+	D+
$2s^2\ 2p^2(^3P)4d\ ^4D_{5/2}$	$2s^2\ 2p^3\ ^4S_{3/2}^o$	905.786	1.657E+07	1.861E+07	-1.913	-1.862	3.647E-02	4.096E-02	0.110	C+	B
$2s^2\ 2p^2(^3P)4d\ ^4D_{3/2}$	$2s^2\ 2p^3\ ^4S_{3/2}^o$	905.834	3.476E+07	3.898E+07	-1.767	-1.717	5.101E-02	5.719E-02	0.108	C+	B
$2s^2\ 2p^2(^3P)4d\ ^4P_{1/2}$	$2s^2\ 2p^3\ ^4S_{3/2}^o$	905.914	5.361E+07	6.005E+07	-1.880	-1.830	3.935E-02	4.407E-02	0.107	C+	B
$2s^2\ 2p^2(^3P)4d\ ^4D_{1/2}$	$2s^2\ 2p^3\ ^4S_{3/2}^o$	906.207	3.201E+07	3.588E+07	-2.103	-2.054	2.352E-02	2.636E-02	0.108	C+	C+
$2s^2\ 2p^2(^3P)4d\ ^4P_{3/2}$	$2s^2\ 2p^3\ ^4S_{3/2}^o$	906.432	4.903E+07	5.510E+07	-1.617	-1.566	7.209E-02	8.101E-02	0.110	C+	B
$2s^2\ 2p^2(^3P)4d\ ^2F_{5/2}$	$2s^2\ 2p^3\ ^4S_{3/2}^o$	906.619	2.562E+07	2.893E+07	-1.722	-1.670	5.655E-02	6.385E-02	0.114	C+	B
$2s^2\ 2p^2(^3P)4d\ ^4P_{5/2}$	$2s^2\ 2p^3\ ^4S_{3/2}^o$	906.731	3.759E+07	4.248E+07	-1.556	-1.503	8.298E-02	9.377E-02	0.115	C+	B
$2s^2\ 2p^2(^3P)4d\ ^2P_{1/2}$	$2s^2\ 2p^3\ ^4S_{3/2}^o$	907.069	1.240E+06	1.416E+06	-3.514	-3.457	9.139E-04	1.043E-03	0.124	C+	D+
...

NOTE— A_B , $\log(gf)_B$, and S_B are, respectively, transition rates, weighted oscillator strengths, and line strengths in the Babushkin (B) form. A_C , $\log(gf)_C$, and S_C are, respectively, transition rates, weighted oscillator strengths, and line strengths in the Coulomb (C) form.

where n is the number of transitions of each group.

As can be seen from Table 5, stronger transitions are usually associated with smaller dT values, while weaker transitions are associated with relatively larger dT values. This is expected since these weaker transitions are mainly unexpected, LS -forbidden E1 transitions, for example, the intercombination transitions and two-electron one-photon transitions, and the challenging nature involved in the computations of these types of transitions due to extensive cancellation between large contributions, see e.g. Ynnerman & Froese Fischer (1995). The cancellation effect can be

Table 5. Statistical results of dT for the computed transition rates. The transitions are divided into five groups based on the magnitude of the A values (in s^{-1}). The number of transitions (No.), the mean dT ($\langle dT \rangle$), and the standard deviations (σ), are given for each group of the transitions. The last three rows show the proportions (in %) of the transitions with dT less than 0.2, 0.1, and 0.05 in all the transitions with $A \geq 10^2 \text{s}^{-1}$.

Group	No.	$\langle dT \rangle$	σ
$< 10^0$	68	65.77	0.35
$10^0 - 10^2$	199	26.65	0.25
$10^2 - 10^4$	422	17.70	0.20
$10^4 - 10^6$	670	9.42	0.12
$> 10^6$	342	4.51	0.08
$dT < 20$		84.31	
$dT < 10$		66.04	
$dT < 5$		51.74	

represented by cancellation factor (CF). Computed line strengths are expected to show large uncertainties when CF is smaller than about 0.1 or 0.05 (Cowan 1981). For LS -allowed transitions computed in this work, 537 out of 905 transitions are associated with CFs large than 0.05, while only 167 out of 796 transitions for LS -forbidden transitions. For most of the strong transitions with $A > 10^6 \text{s}^{-1}$, the mean $\langle dT \rangle$ is less than 0.05 ($\sigma = 0.08$). The proportions of the transitions with different dT values are also statistically analysed and shown in the last three rows: they are 84.3%, 66.0%, and 51.7% for transitions with dT less than 0.2, 0.1, and 0.05, respectively.

Fig. 2 depicts the distributions of the dT values for all the E1 transitions with $A > 10^2 \text{s}^{-1}$. Being consistent with the finding in Table 5, that stronger transitions are associated with smaller dT values and the dT values are within 0.2 for most of the transitions. The mean dT for all presented E1 transitions shown in Fig. 2 is 0.107 ($\sigma = 0.18$).

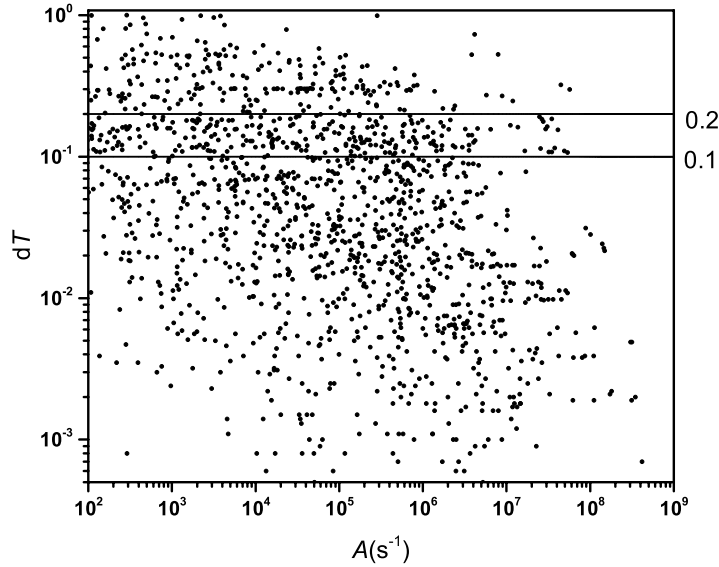


Figure 2. Distributions of dT values along with transition rates A in s^{-1} . The solid lines indicate the 0.1 and 0.2 relative difference between the Babuskin and Coulomb gauges. Note that logarithmic scale is used in both x- and y-axis.

However, the estimation of uncertainties for each transitions is not trivial and there are a number of methods proposed for estimation of uncertainties of calculated transition rates (Kramida 2014; Froese Fischer 2009; Ekman et al. 2014; El-Sayed 2021; Gaigalas et al. 2020). In this work, the estimation of uncertainty is performed by two methods. The first method, which we call $dT\&A$ procedure, is performed in steps as follows: 1. The transitions are

divided in groups based on the A values, i.e. $A < 10^0 \text{ s}^{-1}$, $10^0 \leq A < 10^2 \text{ s}^{-1}$, $10^2 \leq A < 10^3 \text{ s}^{-1}$, $10^3 \leq A < 10^4 \text{ s}^{-1}$, $10^4 \leq A < 10^5 \text{ s}^{-1}$, $10^5 \leq A < 10^7 \text{ s}^{-1}$, and $A \geq 10^7 \text{ s}^{-1}$. 2. The averaged dT_{av} is determined for each group. 3. The related uncertainty percentage for each transition equals $\max(dT, dT_{av})$. The second method employs the procedure from [Kramida \(2013\)](#), which evaluates the accuracy of the computed transition probabilities from comparison of gf_{RCI} and results from NIST-ASD, $gf_{\text{NIST-ASD}}$, and we label it as $gf_{\text{RCI}} \& gf_{\text{NIST-ASD}}$ method. The statistical analysis of the number of transitions belonging to specific accuracy class is performed and the percentage fractions obtained from the above two methods are shown in Figure 3.

For comparison, the percentage fractions in different uncertainty categories obtained from dT values are also shown in Figure 3. We can see that the percentage fraction belonging to high-accuracy class is decreased from 45% by using the dT indicator to 5% using the $dT \& A$ procedure and 0 using the $gf_{\text{RCI}} \& gf_{\text{NIST-ASD}}$ method, which indicates that using the dT values only for accuracy estimations might underestimate the uncertainties. The accuracy classes obtained from $dT \& A$ and $gf_{\text{RCI}} \& gf_{\text{NIST-ASD}}$ methods are given for each transition in the last two columns of Table 4.

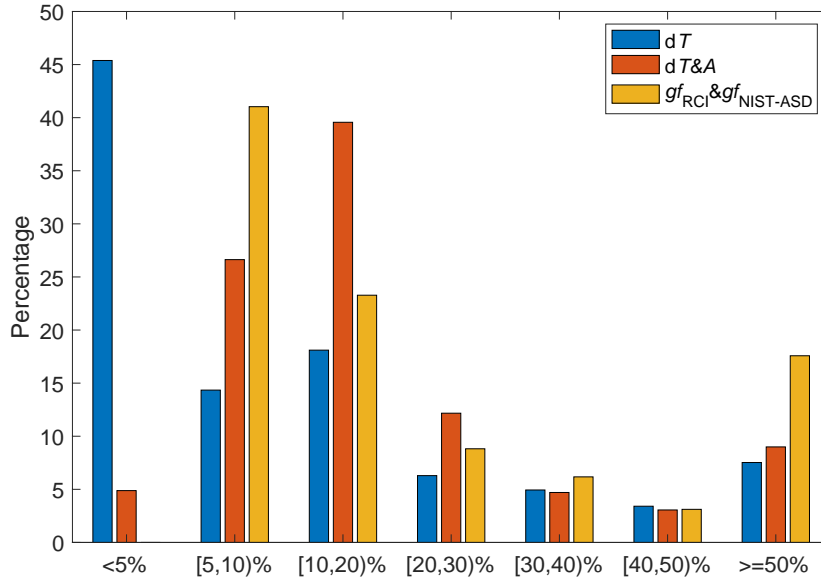


Figure 3. Percentage fractions of all transitions in different uncertainty categories, for the uncertainties based on dT values only (blue), $dT \& A$ procedure (red), and $gf_{\text{RCI}} \& gf_{\text{NIST-ASD}}$ method (yellow) of [Kramida \(2013\)](#).

The accuracy of computed transition parameters can also be estimated by comparisons with previous calculations and experiments. Fig. 4 shows the comparison of the present $\log(gf)$ values and the results from the NIST-ASD. Note that only the values in the NIST-ASD with uncertainties marked C and above are used for comparison. Those NIST-ASD values are compiled by [Wiese et al. \(1996\)](#) and [Wiese & Fuhr \(2007\)](#) based on the results from [Tachiev & Froese Fischer \(2002\)](#); [Musielok et al. \(1995\)](#), and [Hibbert et al. \(1991\)](#). We can see that the agreement between our present computed $\log(gf)$ results and the values from the NIST-ASD is rather good for most of the transitions.

In Fig. 5, we compare our computed $\log(gf)$ values with the results from the other two calculations by [Hibbert et al. \(1991\)](#), performed with the CIV3 code and [Tachiev & Froese Fischer \(2002\)](#), using MCHF-BP method. As is seen in the figure, the differences between the $\log(gf)$ values computed in this work and results from other sources are rather small for most of the transitions. Comparing the present MCDHF/RCI results with those from MCHF-BP calculations by [Tachiev & Froese Fischer \(2002\)](#), which are adopted in the NIST-ASD, 304 (261) out of 334 transitions are in agreement within 25% (10%). The exceptions are the weak transitions with $\log(gf) < -5$. 181 out of 305 transitions are in agreement within 25% with the results from [Hibbert et al. \(1991\)](#). It seems that when both theoretical results, i.e. from [Hibbert et al. \(1991\)](#) and [Tachiev & Froese Fischer \(2002\)](#), are available for the transitions, the present MCDHF/RCI results are in better agreement with the latter.

In Table 6, the computed transition probabilities are compared with the experimental results from [Musielok et al. \(1995\)](#) and [Bridges & Wiese \(2010\)](#). The theoretical results obtained from [Hibbert et al. \(1991\)](#) and [Tachiev](#)

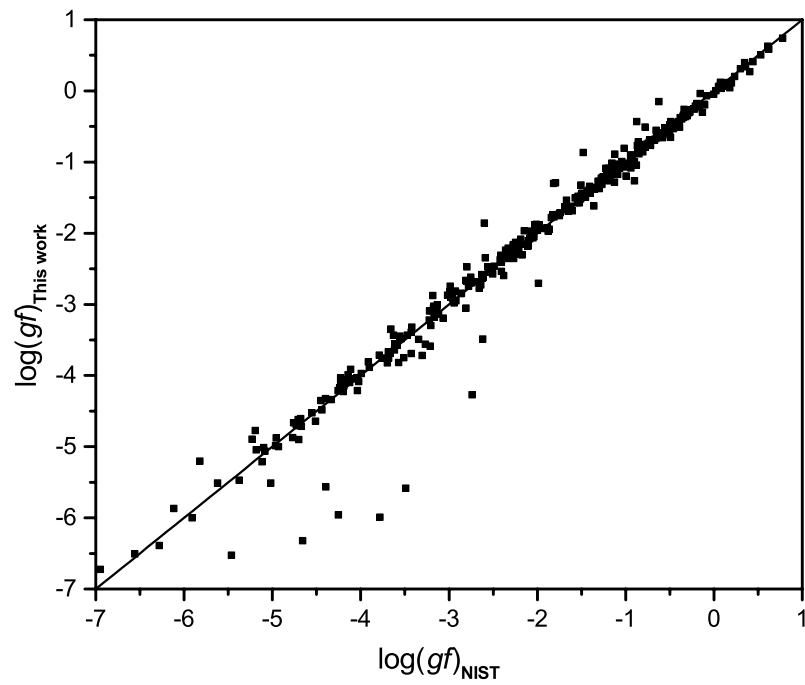


Figure 4. Comparison of the $\log(gf)$ values from the present calculations with the results available in the NIST-ASD.

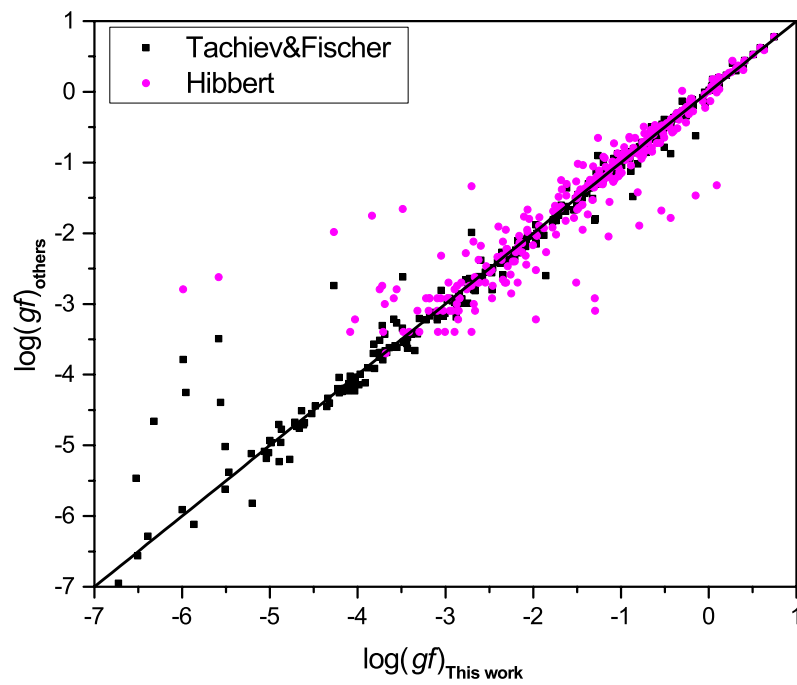


Figure 5. Comparison of the $\log(gf)$ values from the present calculations with the values by Tachiev & Froese Fischer (2002) and Hibbert et al. (1991).

& Froese Fischer (2002), when available, are also listed for comparison. The estimated uncertainties dT of the MCDHF/RCI transition rates are given in parentheses. From Table 6 we can see that when the two experimental results from Musielok et al. (1995) and Bridges & Wiese (2010) are both available for the multiplet, the present results are in slightly better agreement with the latter for the $2p^2(^3P)3p \rightarrow 2p^2(^3P)3s$ transitions, while the situation is getting complex in the case of $2p^2(^3P)3d \rightarrow 2p^2(^3P)3p$ transitions. For allowed $2p^2(^3P)3p \rightarrow 2p^2(^3P)3s$ transitions, present results are in excellent agreement with the two experimental results, as well as with the MCHF-BP (Tachiev & Froese Fischer 2002) and CIV3 (Hibbert et al. 1991) data. While for the $2p^2(^3P)3d \ ^4P \rightarrow 2p^2(^3P)3p \ ^4D^o$ transitions, the present results are in better agreement with the experimental values from Bridges & Wiese (2010) than those from Musielok et al. (1995). For the transitions from $2p^2(^3P)3d \ ^4P_{5/2}$ and $^2F_{5/2}$ levels, the transition rates from the present calculations differ substantially from the experimental values by Bridges & Wiese (2010), that is, by 70%, while the values from (Tachiev & Froese Fischer 2002) appear to be in better agreement with the corresponding experimental results. A closer inspection of the wave function composition given in Table 2 reveals a strong mixing between these two levels. It is very difficult to accurately calculate the radiative properties of such strongly interacting levels.

Table 6. Comparison of transition rates obtained from experimental values with present MCDHF/RCI and other calculations. The present values from MCDHF/RCI calculations are given in the Babushkin gauge. The values in the parentheses are the relative differences between the Babushkin and Coulomb gauges. Note that the values from MCHF calculations are those compiled in the NIST database. The numbers in parentheses without % are the uncertainties with respect to the last digit quoted, for example, 25.31(114) implies 25.31 ± 1.14 .

Transition array	Term	$g_u - g_l$	Transition rate A (10^6 s^{-1})				
			MCDHF/RCI	Tachiev & Fischer ^a	Hibbert et al. ^b	Musielok et al. ^c	Bridges & Wiese ^d
$2p^2(^3P)3p - 2p^2(^3P)3s$	$^4D^o - ^4P$	8 - 6	23.95(1.30%)	25.31(114)	25.96	22.1(24)	23.2(19)
		6 - 4	17.85(1.30%)	18.81(88)	19.25	16.7(18)	17.29(138)
		4 - 2	10.95(1.29%)	11.52(55)	11.79	10.4(11)	10.67(85)
		6 - 6	6.167(1.25%)	6.546(351)	6.725	5.95(71)	5.96(48)
		4 - 4	12.19(1.27%)	12.88(62)	13.20	11.7(13)	12.04(96)
		2 - 2	20.51(1.27%)	21.61(97)	22.11	19.7(22)	20.0(16)
		4 - 6	0.907(1.21%)	0.965(59)	0.993	0.88(12)	
		2 - 4	3.554(1.24%)	3.761(194)	3.857	3.24(39)	3.70(30)
$2p^2(^3P)3p - 2p^2(^3P)3s$	$^4P^o - ^4P$	6 - 6	21.43(1.69%)	22.63(155)	23.07	22.1(27)	
		4 - 4	4.975(1.64%)	5.233(365)	5.312	5.02(60)	
		2 - 2	4.424(1.73%)	4.684(314)	4.771	4.85(58)	
		4 - 6	12.40(1.71%)	13.12(92)	13.41	13.4(16)	
		2 - 4	24.79(1.69%)	26.19(175)	26.67	26.5(32)	
		6 - 4	7.751(1.74%)	8.220(566)	8.385	7.86(94)	
$2p^2(^3P)3p - 2p^2(^3P)3s$	$^4S^o - ^4P$	4 - 2	11.84(1.71%)	12.53(84)	12.74	12.2(15)	
		4 - 6	18.34(0.99%)	19.61(94)	20.17	19.0(21)	17.91(143)
		4 - 4	11.20(0.96%)	11.96(52)	12.36	12.3(14)	11.83(85)
$2p^2(^3P)3p - 2p^2(^3P)3s$	$^2D^o - ^2P$	4 - 2	5.295(0.94%)	5.649(229)	5.856	5.63(62)	5.71(46)
		6 - 4	25.73(0.03%)	25.19(170)	26.79	25.5(31)	
		4 - 2	21.87(0.03%)	21.39(154)	22.63	21.9(26)	
		4 - 4	3.820(0.04%)	3.741(250)	4.043	3.88(50)	

Table 6 continued on next page

Table 6 (*continued*)

Transition array	Term	$g_u - g_l$	Transition rate A (10^6 s^{-1})				
			MCDHF/RCI	Tachiev & Fischer ^a	Hibbert et al. ^b	Musielok et al. ^c	Bridges & Wiese ^d
$2p^2(^3P)3p - 2p^2(^3P)3s$	$^2P^o - ^2P$	4 - 4	26.38(0.35%)	26.78(32)	27.52	25.2(30)	
		2 - 2	20.63(0.37%)	21.45(00)	21.58	19.8(24)	
		2 - 4	10.58(0.32%)	10.75(12)	11.08	9.70(116)	
		4 - 2	4.772(0.37%)	4.871(42)	5.106	4.64(60)	
$2p^2(^3P)4p - 2p^2(^3P)3s$	$^2P^o - ^2P$	4 - 4	1.024(9.36%)			0.749(105)	
		2 - 2	0.895(9.61%)			0.672(94)	
		2 - 4	0.368(8.63%)			0.269(40)	
		4 - 2	0.207(9.67%)			0.240(36)	
$2p^2(^3P)3d - 2p^2(^3P)3p$	$^2P - ^2S^o$	4 - 2	26.19(1.19%)	32.08(590)	32.72	28.7(37)	
		2 - 2	26.02(1.27%)	31.97(583)	32.65	30.0(39)	
$2p^2(^3P)4d - 2p^2(^3P)3p$	$^2P - ^2S^o$	4 - 2	4.054(12.61%)			3.58(50)	
		2 - 2	4.221(12.95%)			3.64(51)	
$2p^2(^3P)3d - 2p^2(^3P)3p$	$^4F - ^4D^o$	10 - 8	36.11(0.98%)	38.96(315)	39.05	37.5(49)	
		8 - 6	31.62(0.98%)	34.11(280)	34.17	31.9(42)	
		6 - 4	27.94(0.97%)	30.15(262)	30.17	28.5(37)	36.9(55)
		4 - 2	25.92(0.98%)	28.05(237)	27.94	26.2(34)	
		8 - 8	3.479(0.90%)	3.833(427)	3.991	3.97(52)	4.42(44)
		6 - 6	6.663(0.99%)	7.317(782)	7.606	7.31(95)	7.58(68)
		4 - 4	9.067(0.96%)	9.833(782)	9.936	9.89(129)	10.3(9)
		6 - 8	0.218(0.01%)	0.239(29)	0.237	0.326(46)	0.256(31)
$2p^2(^3P)3d - 2p^2(^3P)3p$	$^4P - ^4D^o$	6 - 8	0.570(6.85%)	0.822(169)	0.668	1.39(18)	0.842(109)
		4 - 6	0.179(13.75%)	0.223(102)	0.048	0.450(63)	0.236(35)
		2 - 4	0.150(13.72%)	0.183(98)		0.311(44)	0.152(23)
		6 - 6	0.606(2.53%)	1.394(850)	2.471	2.28(30)	1.304(130)
		4 - 4	1.845(2.37%)	2.015(518)	2.787	3.64(47)	2.15(19)
		2 - 2	1.649(3.59%)	1.828(484)	2.999	2.93(38)	1.91(25)
		6 - 4	0.529(0.25%)	0.348(179)	0.332	0.760(106)	0.406(45)
		4 - 2	0.358(1.97%)	0.407(117)	0.707	0.758(106)	0.407(41)
$2p^2(^3P)3d - 2p^2(^3P)3p$	$^4D - ^4D^o$	8 - 8	9.264(1.29%)	10.28(124)	10.02	8.82(115)	
		6 - 6	5.149(1.75%)	5.730(704)	4.900	4.79(62)	
		4 - 4	2.963(2.20%)	3.330(526)	2.408	2.99(39)	
		2 - 2	3.366(2.09%)	3.829(610)	2.640	3.22(42)	
		6 - 8	2.675(0.07%)	2.965(404)	3.243	2.58(34)	
		4 - 6	4.030(0.32%)	4.496(540)	4.717	4.10(53)	
		2 - 4	4.821(0.76%)	5.414(621)	5.603	4.77(62)	
		8 - 6	0.577(1.30%)	0.699(111)	0.751	0.534(75)	
		6 - 4	0.989(1.66%)	1.179(185)	1.115	1.09(14)	
		4 - 2	1.194(1.89%)	1.40(23)	1.151	1.16(15)	

Table 6 *continued on next page*

Table 6 (*continued*)

Transition array	Term	$g_u - g_l$	Transition rate A (10^6 s^{-1})				
			MCDHF/RCI	Tachiev & Fischer ^a	Hibbert et al. ^b	Musielok et al. ^c	Bridges & Wiese ^d
$2p^2(^3P)3d - 2p^2(^3P)3p$	$^4P - ^4P^\circ$	6 - 6	2.976(1.05%)	3.928(159)	3.069	2.37(31)	
		2 - 2	5.353(0.57%)	5.397(924)	9.480	3.39(44)	
		4 - 6	3.721(0.79%)	3.757(363)	2.740	2.29(30)	
		2 - 4	6.649(0.89%)	6.751(701)	4.178	4.01(52)	
		6 - 4	4.829(0.65%)	7.16(160)	10.01	4.18(54)	
		4 - 2	8.942(0.70%)	9.027(793)	11.03	5.55(72)	
$2p^2(^3P)3d - 2p^2(^3P)3p$	$^4D - ^4P^\circ$	8 - 6	24.10(0.27%)	25.46(66)	25.11	23.5(31)	
		6 - 4	12.38(0.18%)	13.20(80)	11.08	12.3(16)	
		4 - 2	6.058(0.10%)	6.541(706)	4.249	6.07(79)	
		6 - 6	11.88(0.43%)	12.35(66)	13.40	11.3(15)	
		4 - 4	15.14(0.36%)	15.91(42)	15.40	15.2(20)	
		2 - 2	17.97(0.25%)	19.11(120)	14.53	17.8(23)	
		4 - 6	3.254(0.48%)	3.332(347)	4.332	3.24(42)	
		2 - 4	7.305(0.42%)	7.553(747)	10.10	7.16(93)	
$2p^2(^3P)5s - 2p^2(^3P)3p$	$^4P - ^4P^\circ$	6 - 6	1.811(8.10%)			1.75(25)	
		4 - 4	0.392(7.87%)			0.445(67)	
		2 - 2	0.348(7.72%)			0.365(55)	
		4 - 6	0.917(7.44%)			0.937(141)	
		2 - 4	1.838(7.46%)			1.94(29)	
		6 - 4	0.758(8.37%)			0.738(111)	
$2p^2(^3P)5s - 2p^2(^3P)3p$	$^2P - ^2D^\circ$	4 - 6	2.252(3.43%)			1.79(25)	
		2 - 4	3.086(7.70%)			2.85(40)	
		4 - 4	0.193(1.44%)			0.230(35)	
$2p^2(^3P)3d - 2p^2(^3P)3p$	$^2F - ^4D^\circ$	6 - 6	1.719(0.57%)	1.064(481)	0.420	2.26(32)	1.34(16)
		8 - 6	0.595(1.00%)	0.609(331)	0.527	1.08(15)	0.646(78)
		6 - 4	0.268(2.32%)	0.485(687)	0.555	0.810(113)	0.462(55)
$2p^2(^3P)3d - 2p^2(^3P)3p$	$^2F - ^4P^\circ$	6 - 4	3.564(0.62%)	1.289(1182)	0.160	1.03(14)	

NOTE—^a Tachiev & Froese Fischer (2002); ^b Hibbert et al. (1991); ^c Musielok et al. (1995); ^d Bridges & Wiese (2010).

As can be seen from Table 6, when three theoretical values are available for the transitions, the present MCDHF/RCI results seem to be in better agreement with the experimental values obtained by Musielok et al. (1995) than the others. 50 out of 72 transitions from present calculations agree with Musielok et al. (1995) within 10%, while 33(37) out of 72 transitions are within the same range for theoretical data from Hibbert et al. (1991)(Tachiev & Froese Fischer (2002)).

There are also a number of measurements of line strength S . In Fig. 6, the selected computed S values are compared with experimental results by Baclawski et al. (2002) and Baclawski & Musielok (2008). The theoretical results of Hibbert et al. (1991) and Froese Fischer & Tachiev (2004) are also shown in the figure. Note that Baclawski et al. (2002) and Baclawski & Musielok (2008) provided the relative line strengths within multiplets (normalized to 100). Therefore, all the theoretical values used for comparison in Fig. 6 are the fractions of line strength for each transition in a multiplet, so that their sum is 100 for each multiplet. The computed S values from present work and the MCHF-BP

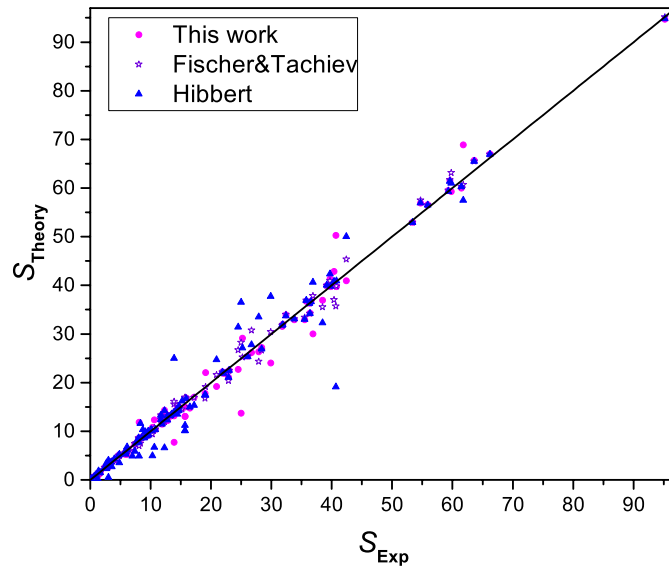


Figure 6. Comparison of the theoretical relative line strengths, S , with the corresponding experimental results published by Baclawski et al. (2002) and Baclawski & Musielok (2008).

calculations by Froese Fischer & Tachiev (2004) are in much better agreement with those experimental values than the CIV3 calculations by Hibbert et al. (1991). The S values from the present work are within the uncertainties of experimental measurements for most of the transitions.

3.3. Validation via the solar spectrum

The Sun is our best understood star, having well constrained parameters (Prša et al. 2016), and for which exist both high quality observations of the emergent intensity (Delbouille & Roland 1995; Neckel 1999; Doerr et al. 2016), as well as realistic simulations of the photospheric layer (Nordlund et al. 2009; Pereira et al. 2013). As such, analyses of the solar intensity spectrum present an alternative way to test the accuracy of the present calculations.

For this purpose we consider the study of Amarsi et al. (2020). The authors presented a detailed analysis of 5 N I lines in the solar disc-center intensity spectrum, using state-of-the-art model atmospheres and radiative transfer methods. From this analysis they measured, for each line as well as the average over all lines, the solar nitrogen abundance, conventionally reported as the logarithmic number density of nitrogen nuclei relative to that of hydrogen nuclei (plus an offset): $A(\text{N}) \equiv \log_{10}(N_{\text{N}}/N_{\text{H}}) + 12$. They adopted the transition probabilities given by Tachiev & Froese Fischer (2002). To first order, their results can be modified to account for new atomic data using

$$A(\text{N})_{\text{new}} = A(\text{N})_{\text{Tachiev}} + \Delta_{\text{new}} \quad (8)$$

where the correction term Δ_{new} is given by

$$\Delta_{\text{new}} = \log(gf)_{\text{Tachiev}} - \log(gf)_{\text{new}}. \quad (9)$$

Table 7 presents the $\log(gf)$ values of the five permitted lines in N I used by (Amarsi et al. 2020). The $\log(gf)$ values in both Coulomb and Babuskin forms from present calculations are given in the table. We can see that for these five transition lines, the present $\log(gf)$ values calculated in the Coulomb and Babuskin agree very well, with the dT values below 0.02. We also investigated the convergence of the wavelengths and oscillator strengths between the results from the calculations of the last two layers. The wavelengths have converged to within 0.1% for all the five transitions and the difference between the oscillator strengths from the calculation of the last two layers is 0.0002 for 744.229 nm, 0.01 for 821.633 nm and 868.34 nm, 0.001 for 862.923 nm, and 0.005 for 1010.89 nm. Experimental measurements of transition probabilities for the lines were reported by Musielok et al. (1995) and Bridges & Wiese (2010); the derived

Table 7. Comparison of the $\log(gf)$ values of the five lines used for abundance analysis in Amarsi et al. (2020). B = Babuskin form and C = Coulomb form.

Upper	Lower	λ_{air}/nm	$\log(gf)$						
			Present		Tachiev	Hibbert	Bautista	Musielok	Bridges
			B	C	& Fischer ^a	et al. ^b	et al. ^c	et al. ^d	& Wiese ^e
$2p^2(^3P)3p^4S_{3/2}^o$	$2p^2(^3P)3s^4P_{3/2}$	744.229	-0.429	-0.433	-0.403	-0.386		-0.39 ± 0.049	-0.41 ± 0.035
$2p^2(^3P)3p^4P_{5/2}^o$	$2p^2(^3P)3s^4P_{5/2}$	821.633	0.116	0.108	0.138	0.147		0.13 ± 0.053	
$2p^2(^3P)3p^2P_{3/2}^o$	$2p^2(^3P)3s^2P_{3/2}$	862.923	0.070	0.068	0.077	0.090	0.057 ± 0.046	0.051 ± 0.052	
$2p^2(^3P)3p^4D_{5/2}^o$	$2p^2(^3P)3s^4P_{3/2}$	868.340	0.084	0.079	0.106	0.116	0.14 ± 0.047	0.054 ± 0.047	0.069 ± 0.035
$2p^2(^3P)3d^4F_{5/2}$	$2p^2(^3P)3p^4D_{3/2}^o$	1010.89	0.410	0.406	0.444	0.443		0.42 ± 0.056	0.53 ± 0.065

NOTE—The table lists: upper and lower configurations along with their spectroscopic terms; wavelengths in air λ_{air} ; weighted oscillator strength $\log(gf)$. ^aTachiev & Froese Fischer (2002); ^bHibbert et al. (1991); ^cBautista et al. (2022); ^dMusielok et al. (1995); ^eBridges & Wiese (2010).

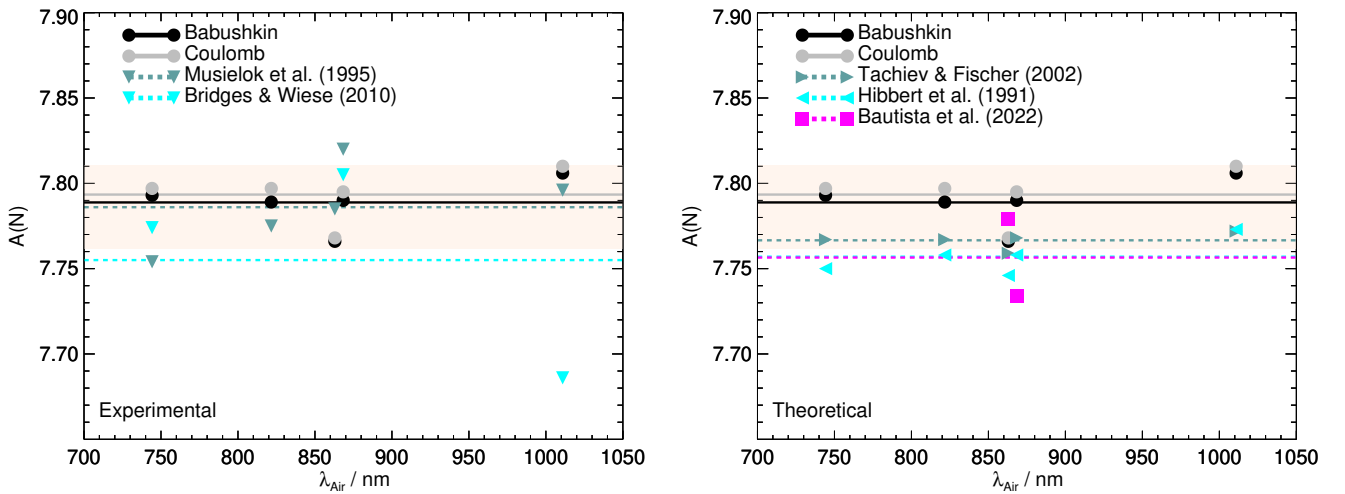


Figure 7. Solar nitrogen abundance inferred using different transition probabilities given in Table 7. Both panels illustrate results based on the theoretical transition data computed in the present work. The left panel also includes results based on the experimental data of Musielok et al. (1995) and Bridges & Wiese (2010), while the right panel includes results based on the theoretical data of Tachiev & Froese Fischer (2002), Hibbert et al. (1991), and Bautista et al. (2022). Horizontal lines show the mean abundance inferred from each data set. In both panels, the shaded region shows the standard deviation of the result based on the experimental data of Musielok et al. (1995), centred on the mean.

$\log(gf)$ values are shown in the last two columns in Table 7. In all cases, our theoretical values and those from Tachiev & Froese Fischer (2002) fall into the range of the estimated uncertainties of the experimental values. The previous calculation by Hibbert et al. (1991) yielded larger $\log(gf)$ values than the experimental determinations for 821.633 nm, 868.340 nm lines while the recommended value for 868.340 nm line by Bautista et al. (2022) is slightly larger than the experimental results.

Fig. 7 compares the data in Table 7 in terms of the solar nitrogen abundance, using Equations 8 and 9. The upper panel compares the results based on the present calculations to the those based on the experimental measurements of both Musielok et al. (1995) and Bridges & Wiese (2010). We see that the mean solar nitrogen abundance from the present calculations (in either gauge) agree well with those from Musielok et al. (1995). Interestingly, this analysis reveals that the transition probability for the 1010.89 nm line from Bridges & Wiese (2010) is significantly overestimated, as it would imply a solar nitrogen abundance significantly lower than what is implied by the other N I lines.

The lower panel of Fig. 7 compares the results based on the present calculations to the those based on the theoretical calculations of Tachiev & Froese Fischer (2002), Hibbert et al. (1991), and Bautista et al. (2022). We see that the mean solar nitrogen abundance from the present calculations (in either gauge) are significantly higher than those from the other three data sets. In particular, this analysis suggests the transition probability for the 868.340 nm line from

Bautista et al. (2022) might be overestimated, as it would imply a solar nitrogen abundance significantly lower than what is implied by the other N I lines, for all of the other theoretical transition probability data sets.

Our new calculations suggest $A(N) = 7.79$ from N I lines, with the results from both the Babushkin gauge and Coulomb gauge in agreement to 0.01 dex. This is an increase of 0.02 dex over the result from Amarsi et al. (2020) based on the transition probabilities given by Tachiev & Froese Fischer (2002). Factoring in also the results from molecular lines ($A(N) = 7.89$; Amarsi et al. 2021), our mean solar nitrogen abundance becomes 7.84, an increase of 0.01 dex over the result given in Asplund et al. (2021). The rather large difference between the abundances inferred from atomic and molecular lines discussed in Amarsi et al. (2021) are thus probably not caused by errors in the N I transition probabilities.

4. CONCLUSIONS

In the present work, MCDHF and complementary RCI calculations have been performed for the lowest 103 states of N I; extending the models of earlier state-of-the-art calculations. Excitation energies, lifetimes, wavelengths, line strengths, transition rates, and weighted oscillator strengths have been systematically computed and provided.

Comparing the excitation energies with experimental data provided by NIST-ASD, the average relative differences of the computed energy levels are 0.07%. The accuracy of the transition data is evaluated based on the relative differences of the computed transition rates in the Coulomb and Babuskin forms, dT , and by extensive comparisons with previous theoretical and experimental results. A statistical analysis of the uncertainties dT of the E1 transitions is performed and the mean dT for transitions with $A > 10^2 \text{ s}^{-1}$ is estimated to be 0.107 ($\sigma = 0.18$), and 0.045 ($\sigma = 0.08$) for transitions with $A > 10^6 \text{ s}^{-1}$. The agreement of the experimental and present theoretical transition properties, for example, oscillator strengths, transition rates, and line strengths, is overall good. But for some weaker transitions, e.g. intercombination transitions, significant discrepancies are present. Such transitions are subject to strong cancellation effects and cannot be properly considered in the present calculations. An improved methodology is needed to further decrease the uncertainties of the respective transition data.

In addition, the present atomic data were employed in an analysis of the solar nitrogen abundance. Our new data suggest a mean solar nitrogen abundance $A(N) = 7.79$ from five N I lines, with the results from both the Babushkin gauge and Coulomb gauge in agreement to 0.01 dex. The new abundance agrees well with that obtained from the experimental measurements of Musielok et al. (1995), while are higher than those from the other theoretical data sets. However, the large difference between the abundances inferred from atomic and molecular lines ($A(N) = 7.89$, Amarsi et al. (2021)) still exists and it is probably not caused by errors in the N I transition probabilities.

- 1 MCL would like to acknowledge the support from the Guangdong Basic and Applied Basic Research Foundation
 2 (2022A1515110043), the Professorial and Doctoral Scientific Research Foundation of Huizhou University No.158020137.
 3 AMA and JG gratefully acknowledge support from the Swedish Research Council (VR 2020-03940, 2020-05467). We
 4 would also like to thank the anonymous referees for their useful comments that helped improve the original manuscript.

REFERENCES

- Aerts, C., Molenberghs, G., Kenward, M. G., & Neiner, C. 2014, *ApJ*, 781, 88, doi: [10.1088/0004-637X/781/2/88](https://doi.org/10.1088/0004-637X/781/2/88)
- Amarsi, A., Grevesse, N., Grumer, J., et al. 2020, *Astronomy & Astrophysics*, 636, A120
- Amarsi, A. M., Grevesse, N., Asplund, M., & Collet, R. 2021, *A&A*, 656, A113, doi: [10.1051/0004-6361/202141384](https://doi.org/10.1051/0004-6361/202141384)
- Amarsi, A. M., Grevesse, N., Grumer, J., et al. 2020, *A&A*, 636, A120, doi: [10.1051/0004-6361/202037890](https://doi.org/10.1051/0004-6361/202037890)
- Asplund, M., Amarsi, A., & Grevesse, N. 2021, *Astronomy & Astrophysics*, 653, A141
- Baclawski, A., & Musielok, J. 2008, *Journal of Quantitative Spectroscopy and Radiative Transfer*, 109, 2537
- . 2010, *Spectrochimica Acta Part B: Atomic Spectroscopy*, 65, 113
- Baclawski, A., Wujec, T., & Musielok, J. 2002, *Physica Scripta*, 65, 28
- Bautista, M. A., Bergemann, M., Carvajal Gallego, H., et al. 2022, arXiv e-prints, arXiv:2206.14095. <https://arxiv.org/abs/2206.14095>
- Belfiore, F., Maiolino, R., Tremonti, C., et al. 2017, *MNRAS*, 469, 151, doi: [10.1093/mnras/stx789](https://doi.org/10.1093/mnras/stx789)
- Bengtsson, G., Larsson, J., Svanberg, S., & Wang, D. 1992, *Physical Review A*, 45, 2712
- Berry, H., Bickel, W., Bashkin, S., Désesquelles, J., & Schectman, R. 1971, *JOSA*, 61, 947

- Bridges, J., & Wiese, W. 2010, *Physical Review A*, 82, 024502
- Bromander, J., Duric, N., Erman, P., & Larsson, M. 1978, *Physica Scripta*, 17, 119, doi: [10.1088/0031-8949/17/2/010](https://doi.org/10.1088/0031-8949/17/2/010)
- Catherinot, A., & Sy, A. 1979, *Physical Review A*, 20, 1511
- Copeland, R. A., Jeffries, J. B., Hickman, A. P., & Crosley, D. R. 1987, *The Journal of chemical physics*, 86, 4876
- Cowan, R. D. 1981, *The theory of atomic structure and spectra No. 3* (Univ of California Press)
- Delbouille, L., & Roland, C. 1995, in *Astronomical Society of the Pacific Conference Series*, Vol. 81, Laboratory and Astronomical High Resolution Spectra, ed. A. J. Sauval, R. Blomme, & N. Grevesse, 32
- Désésquelles, J. 1970, Lyon 1 University, France
- Doerr, H. P., Vitas, N., & Fabbian, D. 2016, *A&A*, 590, A118, doi: [10.1051/0004-6361/201628570](https://doi.org/10.1051/0004-6361/201628570)
- Dumont, P., Biemont, E., & Grevesse, N. 1974, *Journal of Quantitative Spectroscopy and Radiative Transfer*, 14, 1127
- Dyall, K., Grant, I., Johnson, C., Parpia, F., & Plummer, E. 1989, *computer physics communications*, 55, 425
- Ekman, J., Godefroid, M. R., & Hartman, H. 2014, *Atoms*, 2, 215
- El-Sayed, F. 2021, *Journal of Quantitative Spectroscopy and Radiative Transfer*, 276, 107930, doi: <https://doi.org/10.1016/j.jqsrt.2021.107930>
- Esteban, C., Bresolin, F., García-Rojas, J., & Toribio San Cipriano, L. 2020, *Monthly Notices of the Royal Astronomical Society*, 491, 2137
- Froese Fischer, C. 2009, *Physica Scripta*, 2009, 014019
- Froese Fischer, C., Gaigalas, G., Jönsson, P., & Bieroń, J. 2019, *Computer Physics Communications*, 237, 184
- Froese Fischer, C., Godefroid, M., Brage, T., Jönsson, P., & Gaigalas, G. 2016, *Journal of Physics B: Atomic, Molecular and Optical Physics*, 49, 182004
- Froese Fischer, C., & Tachiev, G. 2004, *Atomic Data and Nuclear Data Tables*, 87, 1
- Gaigalas, G., Froese Fischer, C., Rynkun, P., & Jönsson, P. 2017, *Atoms*, 5, 6, doi: [10.3390/atoms5010006](https://doi.org/10.3390/atoms5010006)
- Gaigalas, G., Rynkun, P., Radžiūtė, L., et al. 2020, *The Astrophysical Journal Supplement Series*, 248, 13, doi: [10.3847/1538-4365/ab881a](https://doi.org/10.3847/1538-4365/ab881a)
- Goldbach, C., Lüdtke, T., Martin, M., & Nollez, G. 1992, *Astronomy and Astrophysics*, 266, 605
- Goldbach, C., & Nollez, G. 1991, *Le Journal de Physique IV*, 1, C1
- Grant, I. 1974, *Journal of Physics B: Atomic and Molecular Physics (1968-1987)*, 7, 1458
- Grant, I. P. 2007, *Relativistic quantum theory of atoms and molecules: theory and computation* (Springer)
- Grevesse, N., Lambert, D. L., Sauval, A. J., et al. 1990, *A&A*, 232, 225
- Hibbert, A., Biemont, E., Godefroid, M., & Vaeck, N. 1991, *Astronomy and Astrophysics Supplement Series*, 88, 505
- Hirschi, R. 2007, *A&A*, 461, 571, doi: [10.1051/0004-6361:20065356](https://doi.org/10.1051/0004-6361:20065356)
- Hutchison, R. B. 1971, *Journal of Quantitative Spectroscopy and Radiative Transfer*, 11, 81
- Kolecki, J. R., & Wang, J. 2022, *AJ*, 164, 87, doi: [10.3847/1538-3881/ac7de3](https://doi.org/10.3847/1538-3881/ac7de3)
- Kramida, A. 2013, *Fusion Science and Technology*, 63, 313, doi: [10.13182/FST13-A16437](https://doi.org/10.13182/FST13-A16437)
- Kramida, A. 2014, *Atoms*, 2, 86, doi: [10.3390/atoms2020086](https://doi.org/10.3390/atoms2020086)
- Kramida, A., & Fuhr, J. 2010, NIST atomic transition probability bibliographic database (version 9.0), Online at <https://doi.org/10.18434/T46C7N>, National Institute of Standards and Technology Gaithersburg, MD, USA
- Kramida, A., Yu. Ralchenko, Reader, J., & and NIST ASD Team. 2021, NIST Atomic Spectra Database (ver. 5.9), [Online]. Available: <https://physics.nist.gov/asd> [2022, April 23]. National Institute of Standards and Technology, Gaithersburg, MD.
- Lambert, D. L. 1978, *MNRAS*, 182, 249, doi: [10.1093/mnras/182.2.249](https://doi.org/10.1093/mnras/182.2.249)
- Lawrence, G., & Savage, B. D. 1966, *Physical Review*, 141, 67
- Li, W., Amarsi, A., Papoulia, A., Ekman, J., & Jönsson, P. 2021, *Monthly Notices of the Royal Astronomical Society*, 502, 3780
- Maeder, A., Przybilla, N., Nieva, M.-F., et al. 2014, *A&A*, 565, A39, doi: [10.1051/0004-6361/201220602](https://doi.org/10.1051/0004-6361/201220602)
- Mallow, J., & Burns, J. 1972, *Journal of Quantitative Spectroscopy and Radiative Transfer*, 12, 1081
- Masseron, T., & Gilmore, G. 2015, *MNRAS*, 453, 1855, doi: [10.1093/mnras/stv1731](https://doi.org/10.1093/mnras/stv1731)
- Musielok, J., Wiese, W. L., & Veres, G. 1995, *Physical Review A*, 51, 3588
- Neckel, H. 1999, *SoPh*, 184, 421, doi: [10.1023/A:1017165208013](https://doi.org/10.1023/A:1017165208013)
- Nordlund, Å., Stein, R. F., & Asplund, M. 2009, *Living Reviews in Solar Physics*, 6, 2, doi: [10.12942/lrsp-2009-2](https://doi.org/10.12942/lrsp-2009-2)
- Olsen, J., Roos, B. O., Joergensen, P., & Jensen, H. J. A. 1988, *The Journal of chemical physics*, 89, 2185
- Papoulia, A., Ekman, J., Gaigalas, G., et al. 2019, *Atoms*, 7, 106
- Pereira, T. M. D., Asplund, M., Collet, R., et al. 2013, *A&A*, 554, A118, doi: [10.1051/0004-6361/201321227](https://doi.org/10.1051/0004-6361/201321227)

- Prša, A., Harmanec, P., Torres, G., et al. 2016, *AJ*, 152, 41, doi: [10.3847/0004-6256/152/2/41](https://doi.org/10.3847/0004-6256/152/2/41)
- Przybilla, N., & Butler, K. 2001, *Astronomy & Astrophysics*, 379, 955
- Schiavon, R. P., Zamora, O., Carrera, R., et al. 2017, *MNRAS*, 465, 501, doi: [10.1093/mnras/stw2162](https://doi.org/10.1093/mnras/stw2162)
- Smith, W. H., Bromander, J., Curtis, L., & Buchta, R. 1970, *Physica Scripta*, 2, 211
- Spite, M., Spite, F., Caffau, E., Bonifacio, P., & François, P. 2022, arXiv e-prints, arXiv:2209.10219. <https://arxiv.org/abs/2209.10219>
- Sturesson, L., Jönsson, P., & Froese Fischer, C. 2007, *Computer physics communications*, 177, 539
- Tachiev, G., & Froese Fischer, C. 2002, *Astronomy & Astrophysics*, 385, 716
- Takeda, Y., & Takada-Hidai, M. 1995, *Publications of the Astronomical Society of Japan*, 47, 169
- Tong, M., Froese Fischer, C., & Sturesson, L. 1994, *Journal of Physics B: Atomic, Molecular and Optical Physics*, 27, 4819
- Vincenzo, F., & Kobayashi, C. 2018, *Monthly Notices of the Royal Astronomical Society*, 478, 155
- Wiese, W. L., & Fuhr, J. R. 2007, *Journal of Physical and Chemical Reference Data*, 36, 1287
- Wiese, W. L., Fuhr, J. R., Deters, T. M., et al. 1996, *J. Phys. Chem. Ref. Data*, 7, 157
- Ynnerman, A., & Froese Fischer, C. 1995, *Physical Review A*, 51, 2020